

Combined CDF and DØ measurement of WZ and ZZ production in final states with b -tagged jets

The TEVNPH Working Group*
for the CDF and DØ Collaborations

August 15, 2012

We present a combined measurement of the production cross section of VZ ($V = W$ or Z) events in final states containing charged leptons (electrons or muons) or neutrinos, and heavy flavor jets, using data collected by the CDF and DØ detectors at the Fermilab Tevatron Collider. The analyzed samples of $p\bar{p}$ collisions at $\sqrt{s} = 1.96$ TeV correspond to integrated luminosities of 7.5–9.5 fb^{-1} . Assuming the ratio of the production cross sections $\sigma(WZ)$ and $\sigma(ZZ)$ as predicted by the standard model, we measure the sum of the WZ and ZZ cross sections to be $\sigma(WW+ZZ) = 4.47 \pm 0.64$ (stat) $^{+0.73}_{-0.72}$ (syst) pb. This is consistent with the standard model prediction and corresponds to a significance of 4.6 standard deviations above the background-only hypothesis.

Preliminary Results for the Moriond 2012 Conferences

* The Tevatron New-Phenomena and Higgs Working Group can be contacted at TEVNPHWG@fnal.gov. More information can be found at <http://tevnpwhg.fnal.gov/>.

I. INTRODUCTION

Studies on the production of VV ($V = W, Z$) boson pairs provide an important test of the electroweak sector of the standard model (SM). In $p\bar{p}$ collisions at $\sqrt{s} = 1.96$ TeV, the next-to-leading order (NLO) SM cross sections for these processes are $\sigma(WW) = 11.3 \pm 0.8$ pb, $\sigma(WZ) = 3.2 \pm 0.2$ pb and $\sigma(ZZ) = 1.2 \pm 0.1$ pb [1]. These cross sections assume both γ^* and Z^0 components in the neutral current exchange and corresponding production of dilepton final states in the region $75 \leq m_{\ell\ell} \leq 105$ GeV/ c^2 . Measuring a significant departure in cross section or deviations in the predicted kinematic distributions would indicate the presence of anomalous gauge boson couplings [2] or new particles in extensions of the SM [3]. The VV production in $p\bar{p}$ collisions at the Fermilab Tevatron Collider has been observed in fully leptonic decay modes [4] and in semi-leptonic decay modes [5], where the combined $WW + WZ$ cross section was measured.

Recently, the DØ experiment presented evidence for WZ and ZZ production in semileptonic decays with a b -tagged final state [6]. The WZ and ZZ production cross sections, as well as their sum, were measured in final states where one of the Z bosons decays into $b\bar{b}$ (although there is some signal contribution from $W \rightarrow c\bar{s}$, $Z \rightarrow c\bar{c}$) and the other weak boson decays to charged leptons or neutrinos ($W \rightarrow \ell\nu$, $Z \rightarrow \nu\nu$, or $Z \rightarrow \ell\ell$, with $\ell = e, \mu$). In this note we report an improved measurement of the $WW + ZZ$ production cross section in such final states based on the combination of the DØ results from [6], with a corresponding new set of CDF analyses [7]. This analysis is relevant as a proving ground for the combined Tevatron search for a low-mass Higgs boson produced in association with a weak boson and decaying into a $b\bar{b}$ pair [8] since it shares the same selection criteria as well as analysis and combination techniques.

II. SUMMARY OF CONTRIBUTING ANALYSES

This result is the combination of three CDF analyses [9–11] and three DØ analyses [12–14] outlined in Table I. These analyses utilize data corresponding to integrated luminosities ranging from 7.5 to 9.5 fb $^{-1}$, collected with the CDF [15] and DØ [16] detectors at the Fermilab Tevatron Collider, and they are organized into multiple sub-channels for each different configuration of final state particles. To facilitate proper combination of signals, the analyses from a given experiment are constructed to use mutually exclusive event selections.

In the $\ell\nu b\bar{b}$ analyses [9, 12], events containing an isolated electron or muon, and two or three jets are selected (exactly two jets in the case of the CDF analysis). The presence of a neutrino from the W decay is inferred from a large imbalance of transverse momentum (\cancel{E}_T). The $\nu\nu b\bar{b}$ analyses [10, 13] select events containing large \cancel{E}_T and two or three jets (exactly two jets in the case of the DØ analysis). Finally, in the $\ell\ell b\bar{b}$ analyses [11, 14] events are required to contain two electrons or two muons and at least two jets. In the case of the CDF $\ell\ell b\bar{b}$ analysis, events with two or three jets are analyzed separately. In the DØ $\ell\nu b\bar{b}$ and $\ell\ell b\bar{b}$ analyses as well as the CDF $\ell\ell b\bar{b}$ analysis, each lepton flavor of the W/Z boson decay ($\ell = e, \mu$) is treated as an independent channel. In the case of the CDF $\ell\nu b\bar{b}$ analysis lepton types are separated into four different channels based on their purity and location within the detector. To ensure that event samples used for the different analyses do not overlap, the $\ell\nu b\bar{b}$ analyses reject events in which a second isolated electron or muon is identified, and the $\nu\nu b\bar{b}$ analyses reject events in which any isolated electrons or muons are identified.

To isolate the $Z \rightarrow b\bar{b}$ decays, algorithms for identifying jets consistent with the decay of a heavy-flavor quark are applied to the jets in each event candidate (b -tagging). All of the DØ analyses, as well as the CDF $\ell\nu b\bar{b}$ and $\ell\ell b\bar{b}$ analyses, use multivariate discriminants based on sets of kinematic variables sensitive to displaced decay vertices and tracks within jets with large transverse impact parameters relative to the hard-scatter vertices. The DØ algorithm is a boosted decision tree discriminant which builds upon the previously utilized neural network b -tagging tool [17], while the CDF algorithm [18] is based on a neural network discriminant. In both cases, a spectrum of increasingly stringent b -tagging operating points is constructed through the use of progressively higher requirements on the minimum output of the b -tagging discriminant. The DØ analyses are separated into two groups: a double-tag (DT) group in which two of the jets are b -tagged with a loose tag requirement ($\ell\nu b\bar{b}$ and $\nu\nu b\bar{b}$) or one loose and one tight tag requirement ($\ell\ell b\bar{b}$); and an orthogonal single-tag (ST) group in which only one jet has a loose ($\ell\nu b\bar{b}$ and $\nu\nu b\bar{b}$) or tight ($\ell\ell b\bar{b}$) b -tag. A typical per-jet b efficiency and fake rate for the DØ loose (tight) b -tag selection is about 80% (50%) and 10% (0.5%), respectively. The corresponding efficiency for jets from c -quarks is 45% (12%). The DØ $\ell\nu b\bar{b}$ and $\nu\nu b\bar{b}$ analyses also use the output of the b -tagging algorithm as an additional input to the discriminants used in the final signal extraction. Candidate events in the CDF $\ell\nu b\bar{b}$ and $\ell\ell b\bar{b}$ analyses are also separated into channels based on tight and loose tagging definitions. Events with two tight tags (TT), one tight and one loose tag (TL), two loose tags (LL), and a single tight tag (Tx) are used by both analyses. The CDF $\ell\nu b\bar{b}$ analysis also considers events with a single loose tag (Lx). A typical per-jet efficiency and fake rate for the CDF loose (tight) neural network b -tag selection is about 70% (45%) and 7% (0.6%), respectively. The CDF $\nu\nu b\bar{b}$ analysis utilizes a tight b -tagging algorithm [19] based

on reconstruction of a displaced secondary vertex and a loose b -tagging algorithm [20] that assigns a likelihood for the tracks within a jet to have originated from a displaced vertex. Based on the output of these algorithms events with two tight tags (SS) and those with one tight tag and one loose tag (SJ) are separated into independent analysis channels. The signal in all of the double-tag samples is expected to be primarily composed of events with $Z \rightarrow b\bar{b}$ decays, with smaller contributions from $Z \rightarrow c\bar{c}$ and $W \rightarrow c\bar{s}$ decays. In the single-tag samples, which are defined by less stringent requirements on the b -jet content of the event, the contributions from the three decay modes are comparable.

The primary background is from W/Z +jets, which is modeled with ALPGEN [21] by both CDF and DØ. The backgrounds from multijet production are measured from control samples in the data. At DØ the other backgrounds are generated with ALPGEN and SINGLETOP [22], with PYTHIA [23] providing parton-showering and hadronization. At CDF most backgrounds from other SM processes are modeled using PYTHIA Monte Carlo samples. Background rates are normalized either to next-to-leading order (NLO) or higher-order theory calculations or to data control samples. The DØ $\ell b\bar{b}$ and both experiment's $\ell\nu b\bar{b}$ analyses normalize W/Z +jets backgrounds to data, whereas the the CDF $\ell b\bar{b}$ and both experiment's $\nu\nu b\bar{b}$ analyses normalize them to the predictions from ALPGEN. The fraction of the W/Z +jets in which the jets arise from heavy quarks (b or c) is obtained from NLO calculations using MCFM [24] at DØ while at CDF the prediction from ALPGEN is corrected based on a data control region. The background from $t\bar{t}$ events is normalized to the approximate NNLO cross section [25]. The s -channel and t -channel cross sections for the production of single-top quarks are from approximate NNLO+NNLL calculations [26] and approximate NNNLO+NLL calculations [27], respectively. The background from WW events is normalized to NLO calculations from MCFM [1]. All Monte Carlo samples are passed through detailed GEANT-based simulations [28] of the CDF and DØ detectors.

The DØ analyses use multivariate discriminants (MVA) based on decision trees as the final variables for extracting the VZ signal from the backgrounds. These decision trees are trained to discriminate the VZ signal from the backgrounds using the same set of discriminant variables as in the corresponding Higgs analyses. The CDF analyses follow the same strategy, using neural network-based discriminants instead for signal-to-background discrimination.

III. SYSTEMATIC UNCERTAINTIES

Systematic uncertainties differ between experiments and analyses, and they affect the normalizations and the differential distributions (shapes) of the predicted signal and background templates in correlated ways. The combined result incorporates the sensitivity of predictions to values of nuisance parameters and takes into account correlations in these parameters both within each individual experiment and between experiments. The largest uncertainty contributions and their correlations between and within the two experiments are discussed here. Further details on the individual analyses are available in Refs. [9–14].

1. Correlated Systematics between CDF and DØ

The uncertainties on measurements of the integrated luminosities are 5.9% (CDF) and 6.1% (DØ). Of these values, 4% arises from the uncertainty on the inelastic $p\bar{p}$ scattering cross section, which is correlated between CDF and DØ. CDF and DØ also share the assumed values and uncertainties on the cross sections for WW production and top-quark production processes ($t\bar{t}$ and single top).

In most analyses determination of the multijet (“QCD”) background involves data control samples, and the methods used differ between CDF and DØ, and even between analyses within the collaborations. Therefore, there is no assumed correlation in the predicted rates of this background between analysis channels. Likewise, calibrations of quantities such as the fake lepton rate, b -tag efficiencies, and mistag rates are performed by each collaboration using

TABLE I: List of analysis channels and their corresponding integrated luminosities. See Sect. II for details ($\ell = e, \mu$).

Experiment	Channel	Luminosity (fb ⁻¹)	Reference
CDF	$\ell\nu b\bar{b}$, TT/TL/Tx/LL/Lx, 2 jets	9.5	[9]
CDF	$\nu\nu b\bar{b}$, SS/SJ, 2/3 jets	9.5	[10]
CDF	$\ell b\bar{b}$, TT/TL/Tx/LL, 2/3 jets	9.5	[11]
DØ	$\ell\nu b\bar{b}$, ST/DT, 2/3 jets	7.5	[12]
DØ	$\nu\nu b\bar{b}$, ST/DT, 2 jets	8.4	[13]
DØ	$\ell b\bar{b}$, ST/DT, ≥ 2 jets	7.5	[14]

independent data samples and different methods, and are treated as uncorrelated. Similarly, different techniques are used to estimate background rates for W/Z +heavy flavor backgrounds and the associated uncertainties are taken as uncorrelated.

2. Correlated Systematic Uncertainties for CDF

The dominant systematic uncertainties for the CDF analyses are shown in Appendix Tables II and III for the $\ell\nu b\bar{b}$ channels, in Table IV for the $\nu\nu b\bar{b}$ channels, and in Tables V and VI for the $\ell\ell b\bar{b}$ channels. Each source induces a correlated uncertainty across all of CDF’s channels’ signal and background contributions which are sensitive to that source. The largest uncertainties on signal arise from measured b -tagging efficiencies, jet energy scale, and other Monte Carlo modeling. Shape dependencies of templates on jet energy scale, b -tagging, and gluon radiation (“ISR” and “FSR”) are taken into account for some analyses (see tables). Uncertainties on background event rates vary significantly for the different processes. The backgrounds with the largest systematic rate uncertainties are in general quite small. Such uncertainties are constrained through fits to the nuisance parameters and do not affect the result significantly. Since normalizations for the W/Z +heavy flavor backgrounds are obtained from data in the $\ell\nu b\bar{b}$ and $\nu\nu b\bar{b}$ analyses, the corresponding rate uncertainties associated with each analysis are treated as uncorrelated even within CDF.

3. Correlated Systematic Uncertainties for $D\bar{O}$

The $\nu\nu b\bar{b}$ and $\ell\nu b\bar{b}$ analyses carry an uncertainty on the integrated luminosity of 6.1% [29], while the overall normalization of the $\ell\ell b\bar{b}$ analysis is determined from the NNLO Z/γ^* cross section [30] in data events near the peak of $Z \rightarrow \ell\ell$ decays. The uncertainty from the identification and energy measurement of jets is $\sim 7\%$. The uncertainty arising from the b -tagging rate ranges from 1 to 10%. All analyses include uncertainties associated with lepton measurement and acceptances, which range from 1 to 9% depending on the final state. The largest contribution for all analyses is the theoretical uncertainty on the background cross sections at 7-20% depending on the analysis channel and specific background. The uncertainty on the expected multijet background is dominated by the statistics of the data sample from which it is estimated. Further details on the systematic uncertainties are given in Tables VII-IX. All systematic uncertainties originating from a common source are taken to be 100% correlated, as detailed in Table X.

IV. MEASUREMENT OF THE $WZ + ZZ$ CROSS SECTION

The total VZ cross section is determined from a maximum likelihood fit of the MVA distributions for the background and signal samples from the contributing analyses to the data. The cross section for the signal ($WZ + ZZ$) is a free parameter in the fit, but the ratio of the WZ and ZZ cross sections is fixed to the SM prediction. Events from WW production are considered as a background. The fit is performed simultaneously on the distributions in all sub-channels. As a consistency check, we also determine the Bayesian posterior probability by integrating over the nuisance parameters. Here we report only the results from the maximum likelihood fit, but the results from the Bayesian method are consistent.

The combined fit for the total VZ cross section distributions yields $\sigma(WW+WZ) = 4.47 \pm 0.64$ (stat) $^{+0.73}_{-0.72}$ (syst) pb. This measurement is consistent with the NLO SM prediction of $\sigma(WW + WZ) = 4.4 \pm 0.3$ pb [1], as well as with the individual measurements from $D\bar{O}$ [6], $\sigma(WW + WZ) = 5.0 \pm 1.6$ pb, and from CDF [7], $\sigma(WW + WZ) = 4.1^{+1.4}_{-1.3}$ pb. Based on the measured central value for the VZ cross section and its uncertainties, the observed significance is estimated to be 4.6 standard deviations (s.d.), while the expected significance is ~ 4.8 s.d.

To visualize the sensitivity of the combined analysis, we calculate the expected signal over background (s/b) in each bin of the MVA distributions from the contributing analyses. Bins with similar s/b are then combined to produce a single distribution, shown in Fig. 1. The binning was chosen to keep the background fluctuations roughly of the same size as in the dijet mass distributions. Figure 2 shows the distributions of the invariant mass of the dijet system, summed over all channels from CDF and $D\bar{O}$, after adjusting the signal and background predictions according to the results of the fit. Figure 3 shows the background subtracted dijet mass distributions after the fit, demonstrating the presence of a hadronic resonance in the data consistent with the SM expectation, both in shape and normalization.

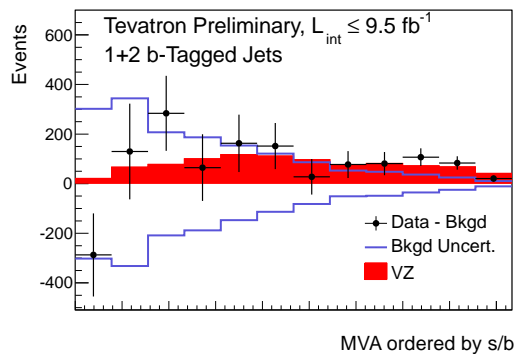


FIG. 1: Comparison of the measured VZ signal (filled histogram) to background-subtracted data (points) after the maximum likelihood fit. The distribution is a combination of all final discriminants where the bins are ordered and merged according to their expected signal to background ratio (s/b). The x -axis has arbitrary units. Also shown is the ± 1 standard deviation uncertainty on the fitted background that was subtracted.

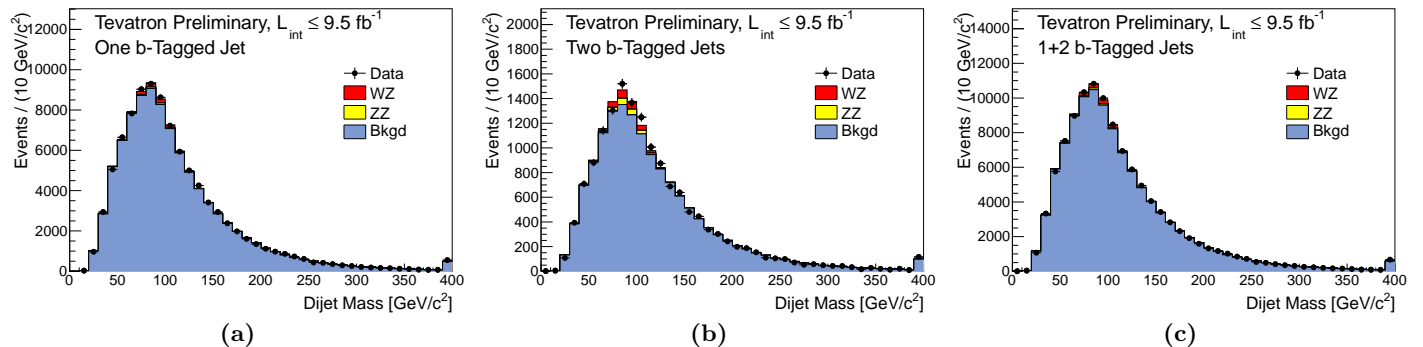


FIG. 2: Comparison of the fitted signal+background to data in the dijet mass distribution (summed over all channels) for the (a) ST, and (b) DT sub-channels; and (c) the sum of the ST and DT sub-channels. Events with a dijet mass greater than 400 GeV are included in the last bin of the distribution.

V. SUMMARY

In summary, we combine analyses in the $\ell\nu b\bar{b}$, $\nu\nu b\bar{b}$, and $\ell\ell b\bar{b}$ ($\ell = e, \mu$) final states from the CDF and DØ experiments to observe, with a significance of 4.6 s.d., the production of VZ ($V = W$ or Z) events. The analyzed samples correspond to 7.5 to 9.5 fb^{-1} of $p\bar{p}$ collisions at $\sqrt{s} = 1.96 \text{ TeV}$. We measure the total cross section for VZ production to be $\sigma(WW + WZ) = 4.47 \pm 0.64$ (stat) $^{+0.73}_{-0.72}$ (syst) pb. This result demonstrates the ability of the Tevatron experiments to measure a SM production process with cross section of the same order magnitude as that expected for Higgs production from the same set of background-dominated final states containing two heavy-flavor jets used in our low mass Higgs searches.

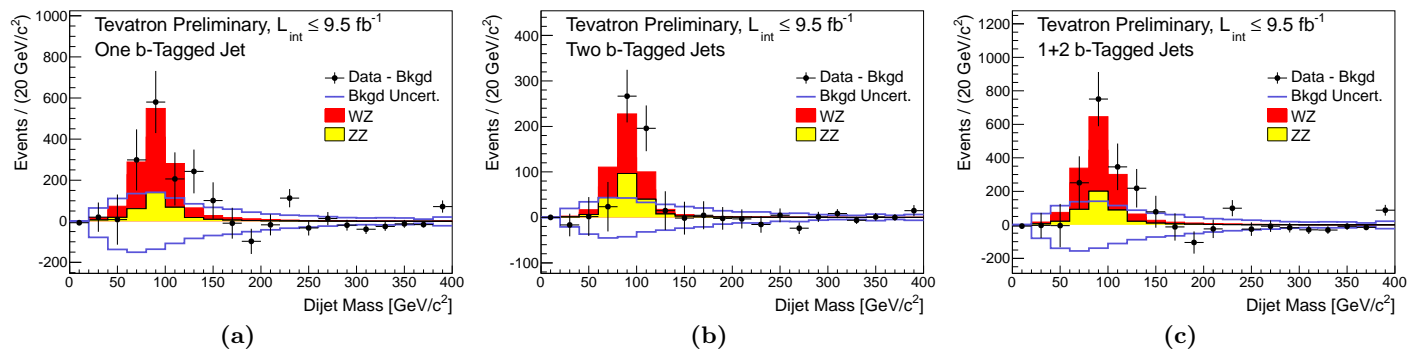


FIG. 3: Comparison of the measured WZ and ZZ signals (filled histograms) to background-subtracted data (points) in the dijet mass distribution (summed over all channels) for the (a) ST, and (b) DT sub-channels; and (c) the sum of the ST and DT sub-channels. Also shown is the ± 1 standard deviation uncertainty on the fitted background. Events with a dijet mass greater than 400 GeV are included in the last bin of the distribution.

Acknowledgments

We thank the Fermilab staff and the technical staffs of the participating institutions for their contributions, and we acknowledge support from the DOE and NSF (USA); CONICET and UBACyT (Argentina); ARC (Australia); CNPq, FAPERJ, FAPESP and FUNDUNESP (Brazil); CRC Program and NSERC (Canada); CAS, CNSF, and NSC (China); Colciencias (Colombia); MSMT and GACR (Czech Republic); Academy of Finland (Finland); CEA and CNRS/IN2P3 (France); BMBF and DFG (Germany); INFN (Italy); DAE and DST (India); SFI (Ireland); Ministry of Education, Culture, Sports, Science and Technology (Japan); KRF, KOSEF and World Class University Program (Korea); CONACyT (Mexico); FOM (The Netherlands); FASI, Rosatom and RFBR (Russia); Slovak R&D Agency (Slovakia); Ministerio de Ciencia e Innovación, and Programa Consolider-Ingenio 2010 (Spain); The Swedish Research Council (Sweden); Swiss National Science Foundation (Switzerland); STFC and the Royal Society (United Kingdom); and the A.P. Sloan Foundation (USA).

-
- [1] J. M. Campbell and R. K. Ellis, Phys. Rev. D **60**, 113006 (1999). We used MCFM v6.0. Cross sections are computed using a choice of scale $\mu_0^2 = M_V^2 + p_T^2(V)$, where V is the vector boson, and the MSTW2008 PDF set.
- [2] K. Hagiwara, S. Ishihara, R. Szalapski, and D. Zeppenfeld, Phys. Rev. D **48** (1993).
- [3] J. C. Pati and A. Salam, Phys. Rev. D **10**, 275 (1974); **11** 703(E) (1975);
G. Altarelli, B. Mele, and M. Ruiz-Altaba, Z. Phys. C **45**, 109 (1989); **47**, 676(E) (1990);
L. Randall and R. Sundrum, Phys. Rev. Lett. **83**, 3370 (1999);
H. Davoudiasl, J. L. Hewett, and T. G. Rizzo, Phys. Rev. D **63**, 075004 (2001);
H. He *et al.*, Phys. Rev. D **78**, 031701 (2008).
- [4] T. Aaltonen *et al.* (CDF Collaboration), Phys. Rev. Lett. **104**, 201801 (2010);
V. M. Abazov *et al.* (D0 Collaboration), Phys. Rev. Lett. **101**, 171803 (2008);
V. M. Abazov *et al.* (D0 Collaboration), Phys. Lett. B **695**, 67 (2011);
V. M. Abazov *et al.* (D0 Collaboration), Phys. Rev. D **84**, 011103 (2011);
V. M. Abazov *et al.* (D0 Collaboration), arXiv:1201.5652 [hep-ex].
- [5] T. Aaltonen *et al.* (CDF Collaboration), Phys. Rev. Lett. **103**, 091803 (2009);
T. Aaltonen *et al.* (CDF Collaboration), Phys. Rev. Lett. **104**, 101801 (2010);
V. M. Abazov *et al.* (D0 Collaboration), arXiv:1112.0536 [hep-ex].
- [6] V. M. Abazov *et al.* (D0 Collaboration), DØ Note 6260-CONF (2011).
- [7] T. Aaltonen *et al.* (CDF Collaboration), CDF Conference Note 10805 (2012).
- [8] V. M. Abazov *et al.* (D0 Collaboration), Phys. Rev. Lett. **104**, 071801 (2010);
V. M. Abazov *et al.* (D0 Collaboration), Phys. Rev. Lett. **105**, 251801 (2010);
V. M. Abazov *et al.* (D0 Collaboration), Phys. Lett. B **698**, 6 (2011);
T. Aaltonen *et al.* (CDF Collaboration), Phys. Rev. Lett. **105**, 251802 (2010);
T. Aaltonen *et al.* (CDF Collaboration), Phys. Rev. Lett. **103**, 101802 (2009);
T. Aaltonen *et al.* (CDF Collaboration), Phys. Rev. Lett. **104**, 141801 (2010).
- [9] T. Aaltonen *et al.* (CDF Collaboration), CDF Conference Note 10796 (2012).
- [10] T. Aaltonen *et al.* (CDF Collaboration), CDF Conference Note 10798 (2012).
- [11] T. Aaltonen *et al.* (CDF Collaboration), CDF Conference Note 10799 (2012).
- [12] V. M. Abazov *et al.* (D0 Collaboration), DØ Note 6220-CONF (2011).
- [13] V. M. Abazov *et al.* (D0 Collaboration), DØ Note 6223-CONF (2011).
- [14] V. M. Abazov *et al.* (D0 Collaboration), DØ Note 6256-CONF (2011).
- [15] D. Acosta *et al.* (CDF Collaboration), Phys. Rev. D **71**, 032001 (2005).
- [16] V. M. Abazov *et al.* (D0 Collaboration), Nucl. Instrum. Methods Phys. Res. A **565**, 463 (2006);
M. Abolins *et al.*, Nucl. Instrum. Methods Phys. Res. A **584**, 75 (2008);
R. Angstadt *et al.*, Nucl. Instrum. Methods Phys. Res. A **622**, 298 (2010).
- [17] V. M. Abazov *et al.* (D0 Collaboration), Nucl. Instrum. Methods Phys. Res. A **620**, 490 (2010).
- [18] T. Aaltonen *et al.* (CDF Collaboration), CDF Conference Note 10803 (2012).
- [19] D. Acosta *et al.* (CDF Collaboration), Phys. Rev. D **71**, 052003 (2005).
- [20] A. Abulencia *et al.* (CDF and CDF - Run II Collaborations), Phys. Rev. D **74**, 072006 (2006).
- [21] M. L. Mangano, M. Moretti, F. Piccinini, R. Pittau and A. D. Polosa, J. High Energy Phys. **07**, 001 (2003).
- [22] CompHEP, E. Boos *et al.*, Nucl. Instrum. Methods Phys. Res. A **534**, 250 (2004);
E. Boos, V. Bunichev, L. Dudko, V. Savrin, and A. Sherstnev, Phys. Atom. Nucl. **69**, 1317 (2006).
- [23] T. Sjöstrand, L. Lonnblad and S. Mrenna, arXiv:hep-ph/0108264.
- [24] J. M. Campbell and R. K. Ellis, <http://mcfm.fnal.gov/>.
J. M. Campbell, R. K. Ellis, Nucl. Phys. Proc. Suppl. **205-206**, 10 (2010).
- [25] U. Langenfeld, S. Moch and P. Uwer, Phys. Rev. D **80**, 054009 (2009).
- [26] N. Kidonakis, arXiv:1005.3330 [hep-ph] (2010);
N. Kidonakis, Phys. Rev. D **81**, 054028 (2010).
- [27] N. Kidonakis, Phys. Rev. D **74**, 114012 (2006).
- [28] R. Brun, R. Hagelberg, M. Hansroul, and J. C. Lasalle, *GEANT: Simulation Program for Particle Physics Experiments. User Guide and Reference Manual*, CERN-DD-78-2-REV;
S. Agostinelli *et al.*, Nucl. Instrum. Methods A **506**, 250 (2003).
- [29] T. Andeen *et al.*, FERMILAB-TM-2365 (2007).
- [30] R. Hamberg, W.L. van Neerven and W.B. Kilgore, Nucl Phys. B **359**, 343 (1991) [Erratum-ibid. B **644**, 403 (2002)].
- [31] T. Junk, Nucl. Instrum. Methods Phys. Res. A **434**, 435 (1999);
A. L. Read, J. Phys. G **28**, 2693 (2002).
- [32] W. Fisher, FERMILAB-TM-2386-E (2006).

Appendix A: Additional Material

TABLE II: Systematic uncertainties for the CDF $\ell\nu b\bar{b}$ single tight tag (Tx) and single loose tag (Lx) channels. Systematic uncertainties are listed by name; see the original references for a detailed explanation of their meaning and on how they are derived. Uncertainties are relative, in percent on the event yield. Shape uncertainties are labeled with an “(S)”.

CDF $\ell\nu b\bar{b}$ single tight tag (Tx) channels relative uncertainties (%)

Contribution	$W+HF$	Mistags	Top	Diboson	Non- W	WH
Luminosity ($\sigma_{\text{inel}}(p\bar{p})$)	3.8	0	3.8	3.8	0	3.8
Luminosity Monitor	4.4	0	4.4	4.4	0	4.4
Lepton ID	2.0-4.5	0	2.0-4.5	2.0-4.5	0	2.0-4.5
Jet Energy Scale	3.2-6.9(S)	0.9-1.8(S)	0.8-9.7(S)	3.6-13.2(S)	0	3.0-5.0(S)
Mistag Rate (tight)	0	19	0	0	0	0
Mistag Rate (loose)	0	0	0	0	0	0
B -Tag Efficiency (tight)	0	0	3.9	3.9	0	3.9
B -Tag Efficiency (loose)	0	0	0	0	0	0
$t\bar{t}$ Cross Section	0	0	10	0	0	0
Diboson Rate	0	0	0	6.0	0	0
Signal Cross Section	0	0	0	0	0	5
HF Fraction in W +jets	30	0	0	0	0	0
ISR+FSR+PDF	0	0	0	0	0	3.8-6.8
Q^2	3.2-6.9(S)	0.9-1.8(S)	0	0	0	0
QCD Rate	0	0	0	0	40	0

CDF $\ell\nu b\bar{b}$ single loose tag (Lx) channels relative uncertainties (%)

Contribution	$W+HF$	Mistags	Top	Diboson	Non- W	WH
Luminosity ($\sigma_{\text{inel}}(p\bar{p})$)	3.8	0	3.8	3.8	0	3.8
Luminosity Monitor	4.4	0	4.4	4.4	0	4.4
Lepton ID	2	0	2	2	0	2
Jet Energy Scale	2.2-6.0(S)	0.9-1.8(S)	1.6-8.6(S)	4.6-9.6(S)	0	3.1-4.8(S)
Mistag Rate (tight)	0	0	0	0	0	0
Mistag Rate (loose)	0	10	0	0	0	0
B -Tag Efficiency (tight)	0	0	0	0	0	0
B -Tag Efficiency (loose)	0	0	3.2	3.2	0	3.2
$t\bar{t}$ Cross Section	0	0	10	0	0	0
Diboson Rate	0	0	0	6.0	0	0
Signal Cross Section	0	0	0	0	0	10
HF Fraction in W +jets	30	0	0	0	0	0
ISR+FSR+PDF	0	0	0	0	0	2.4-4.9
QCD Rate	2.1-6.0(S)	0.9-1.8(S)	0	0	40	0

TABLE III: Systematic uncertainties for the CDF $\ell\nu b\bar{b}$ double tight tag (TT), one tight tag and one loose tag (TL) and double loose tag (LL) channels. Systematic uncertainties are listed by name; see the original references for a detailed explanation of their meaning and on how they are derived. Uncertainties are relative, in percent on the event yield. Shape uncertainties are labeled with an “(S)”.

CDF $\ell\nu b\bar{b}$ double tight tag (TT) channels relative uncertainties (%)

Contribution	W+HF	Mistags	Top	Diboson	Non-W	WH
Luminosity ($\sigma_{\text{inel}}(pp)$)	3.8	0	3.8	3.8	0	3.8
Luminosity Monitor	4.4	0	4.4	4.4	0	4.4
Lepton ID	2.0-4.5	0	2.0-4.5	2.0-4.5	0	2.0-4.5
Jet Energy Scale	4.0-16.6(S)	0.9-3.3(S)	0.9-10.4(S)	4.7-19.7(S)	0	2.3-13.6(S)
Mistag Rate (tight)	0	40	0	0	0	0
Mistag Rate (loose)	0	0	0	0	0	0
B-Tag Efficiency (tight)	0	0	7.8	7.8	0	7.8
B-Tag Efficiency (loose)	0	0	0	0	0	0
$t\bar{t}$ Cross Section	0	0	10	0	0	0
Diboson Rate	0	0	0	6.0	0	0
Signal Cross Section	0	0	0	0	0	5
HF Fraction in W+jets	30	0	0	0	0	0
ISR+FSR+PDF	0	0	0	0	0	6.4-12.6
Q^2	4.0-8.8(S)	0.9-1.8(S)	0	0	0	0
QCD Rate	0	0	0	0	40	0

CDF $\ell\nu b\bar{b}$ one tight and one loose tag (TL) channels relative uncertainties (%)

Contribution	W+HF	Mistags	Top	Diboson	Non-W	WH
Luminosity ($\sigma_{\text{inel}}(pp)$)	3.8	0	3.8	3.8	0	3.8
Luminosity Monitor	4.4	0	4.4	4.4	0	4.4
Lepton ID	2.0-4.5	0	2.0-4.5	2.0-4.5	0	2.0-4.5
Jet Energy Scale	3.9-12.4(S)	0.9-3.3(S)	1.4-11.5(S)	5.0-16.0(S)	0	2.5-16.1(S)
Mistag Rate (tight)	0	19	0	0	0	0
Mistag Rate (loose)	0	10	0	0	0	0
B-Tag Efficiency (tight)	0	0	3.9	3.9	0	3.9
B-Tag Efficiency (loose)	0	0	3.2	3.2	0	3.2
$t\bar{t}$ Cross Section	0	0	10	0	0	0
Diboson Rate	0	0	0	6.0	0	0
Signal Cross Section	0	0	0	0	0	5
HF Fraction in W+jets	30	0	0	0	0	0
ISR+FSR+PDF	0	0	0	0	0	3.3-10.3
Q^2	3.9-7.7(S)	0.9-1.9(S)	0	0	0	0
QCD Rate	0	0	0	0	40	0

CDF $\ell\nu b\bar{b}$ one tight and one loose tag (TL) channels relative uncertainties (%)

Contribution	W+HF	Mistags	Top	Diboson	Non-W	WH
Luminosity ($\sigma_{\text{inel}}(pp)$)	3.8	0	3.8	3.8	0	3.8
Luminosity Monitor	4.4	0	4.4	4.4	0	4.4
Lepton ID	2	0	2	2	0	2
Jet Energy Scale	3.6-6.9(S)	0.9-1.8(S)	1.7-7.9(S)	1.2-8.5	0	2.7-5.4(S)
Mistag Rate (tight)	0	0	0	0	0	0
Mistag Rate (loose)	0	20	0	0	0	0
B-Tag Efficiency (tight)	0	0	0	0	0	0
B-Tag Efficiency (loose)	0	0	6.3	6.3	0	6.3
$t\bar{t}$ Cross Section	0	0	10	0	0	0
Diboson Rate	0	0	0	6.0	0	0
Signal Cross Section	0	0	0	0	0	10
HF Fraction in W+jets	30	0	0	0	0	0
ISR+FSR+PDF	0	0	0	0	0	2.0-13.6
QCD Rate	3.6-6.9(S)	0.9-1.8(S)	0	0	40	0

TABLE IV: Systematic uncertainties for the CDF $\nu\nu b\bar{b}$ tight double tag (SS) and loose double tag (SJ) channels. Systematic uncertainties are listed by name; see the original references for a detailed explanation of their meaning and on how they are derived. Uncertainties are relative, in percent on the event yield. Shape uncertainties are labeled with an “(S)”.

CDF $\nu\nu b\bar{b}$ tight double tag (SS) channel relative uncertainties (%)									
Contribution	ZH	WH	Multijet	Mistags	Top Pair	S. Top	Diboson	W + HF	Z + HF
Luminosity	3.8	3.8			3.8	3.8	3.8	3.8	3.8
Lumi Monitor	4.4	4.4			4.4	4.4	4.4	4.4	4.4
Tagging SF	10.4	10.4			10.4	10.4	10.4	10.4	10.4
Trigger Eff. (S)	0.9	1.4	0.9		0.9	1.6	2.0	1.8	1.2
Lepton Veto	2.0	2.0			2.0	2.0	2.0	2.0	2.0
PDF Acceptance	3.0	3.0			3.0	3.0	3.0	3.0	3.0
JES (S)	+1.7 -1.8	+2.4 -2.3			+0.0 -0.1	+2.5 -2.4	+4.1 -4.5	+4.3 -4.6	+8.8 -3.2
ISR/FSR		+3.0 +3.0							
Cross-Section	5	5			10	10	6	30	30
Multijet Norm. (shape)			2.5						
Mistag (S)				+36.7 -30					

CDF $\nu\nu b\bar{b}$ loose double tag (SJ) channel relative uncertainties (%)									
Contribution	ZH	WH	Multijet	Mistags	Top Pair	S. Top	Diboson	W + HF	Z + HF
Luminosity	3.8	3.8			3.8	3.8	3.8	3.8	3.8
Lumi Monitor	4.4	4.4			4.4	4.4	4.4	4.4	4.4
Tagging SF	8.3	8.3			8.3	8.3	8.3	8.3	8.3
Trigger Eff. (S)	1.2	1.7	1.6		0.9	1.8	2.0	2.5	1.9
Lepton Veto	2.0	2.0			2.0	2.0	2.0	2.0	2.0
PDF Acceptance	3.0	3.0			3.0	3.0	3.0	3.0	3.0
JES (S)	+1.9 -1.9	+2.4 -2.4			+3.0 -2.8	-0.6 0.2	+4.2 -4.2	+6.8 -5.9	+8.3 -3.1
ISR/FSR		+2.4 -2.4							
Cross-Section	5.0	5.0			10	10	6	30	30
Multijet Norm.			1.6						
Mistag (S)				+65.2 -38.5					

TABLE VII: Systematic uncertainties for the D0 $\ell\nu b\bar{b}$ single tag (ST) and double tag (DT) channels. Systematic uncertainties are listed by name; see the original references for a detailed explanation of their meaning and on how they are derived. Uncertainties are relative, in percent on the event yield. Shape uncertainties are labeled with an “(S)”, and “SO” represents uncertainties that affect only the shape, but not the event yield.

D0 $\ell\nu b\bar{b}$ Single Tag (ST) channels relative uncertainties (%)

Contribution	Dibosons	$W + b\bar{b}/c\bar{c}$	$W+l.f.$	$t\bar{t}$	single top	Multijet
Luminosity	6.1	6.1	6.1	6.1	6.1	–
Electron ID/Trigger efficiency (S)	1–5	2–4	2–4	1–2	1–2	–
Muon Trigger efficiency (S)	1–3	1–2	1–3	2–5	2–3	–
Muon ID efficiency/resolution	4.1	4.1	4.1	4.1	4.1	–
Jet ID efficiency (S)	2–5	1–2	1–3	3–5	2–4	–
Jet Energy Resolution (S)	4–7	1–3	1–4	2–5	2–4	–
Jet Energy Scale (S)	4–7	2–5	2–5	2–5	2–4	–
Vertex Conf. Jet (S)	4–10	5–12	4–10	7–10	5–10	–
b -tag/taggability (S)	1–4	1–2	3–7	3–5	1–2	–
Heavy-Flavor K-factor	–	20	–	–	–	–
Multijet model, $e\nu b\bar{b}$ (S)	1–2	2–4	1–3	1–2	1–3	15
Multijet model, $\mu\nu b\bar{b}$	–	2.4	2.4	–	–	20
Cross Section	6	9	9	10	10	–
ALPGEN MLM pos/neg(S)	–	SO	–	–	–	–
ALPGEN Scale (S)	–	SO	SO	–	–	–
Underlying Event (S)	–	SO	–	–	–	–
PDF, reweighting	2	2	2	2	2	–

D0 $\ell\nu b\bar{b}$ Double Tag (DT) channels relative uncertainties (%)

Contribution	Dibosons	$W + b\bar{b}/c\bar{c}$	$W+l.f.$	$t\bar{t}$	single top	Multijet
Luminosity	6.1	6.1	6.1	6.1	6.1	–
Electron ID/Trigger efficiency (S)	2–5	2–3	2–3	1–2	1–2	–
Muon Trigger efficiency (S)	2–4	1–2	1–2	2–4	1–3	–
Muon ID efficiency/resolution	4.1	4.1	4.1	4.1	4.1	–
Jet ID efficiency (S)	2–8	2–5	4–9	3–7	2–4	–
Jet Energy Resolution (S)	4–7	2–7	2–7	2–9	2–4	–
Jet Energy Scale (S)	4–7	2–6	2–7	2–6	2–7	–
Vertex Conf. Jet (S)	4–10	5–12	4–10	7–10	5–10	–
b -tag/taggability (S)	3–7	4–6	3–10	5–10	4–10	–
Heavy-Flavor K-factor	–	20	–	–	–	–
Multijet model, $e\nu b\bar{b}$ (S)	1–2	2–4	1–3	1–2	1–3	15
Multijet model, $\mu\nu b\bar{b}$	–	2.4	2.4	–	–	20
Cross Section	6	9	9	10	10	–
ALPGEN MLM pos/neg(S)	–	SO	–	–	–	–
ALPGEN Scale (S)	–	SO	SO	–	–	–
Underlying Event (S)	–	SO	–	–	–	–
PDF, reweighting	2	2	2	2	2	–

TABLE VIII: Systematic uncertainties for the D0 $\nu\nu b\bar{b}$ single tag (ST) and double tag (DT) channels. Systematic uncertainties are listed by name; see the original references for a detailed explanation of their meaning and on how they are derived. Uncertainties are relative, in percent on the event yield. Shape uncertainties are labeled with an “(S)”, and “SO” represents shape only uncertainty.

D0 $\nu\nu b\bar{b}$ Single Tag (ST) channels relative uncertainties (%)

Contribution	Top	$V + b\bar{b}/c\bar{c}$	$V+l.f.$	Dibosons	Multijet
Jet ID efficiency (S)	2.0	2.0	2.0	2.0	–
Jet Energy Scale (S)	2.2	1.6	3.1	1.0	–
Jet Energy Resolution (S)	0.5	0.3	0.3	0.9	–
Vertex Conf. / Taggability (S)	3.2	1.9	1.7	1.8	–
b Tagging (S)	1.1	0.8	1.8	1.2	–
Lepton Identification	1.6	0.9	0.8	1.0	–
Trigger	2.0	2.0	2.0	2.0	–
Heavy Flavor Fractions	–	20.0	–	–	–
Multijet model	–	–	–	–	25
Cross Sections	10.0	10.2	10.2	7.0	–
Luminosity	6.1	6.1	6.1	6.1	–
Multijet Normalilzation	–	–	–	–	–
ALPGEN MLM (S)	–	–	SO	–	–
ALPGEN Scale (S)	–	SO	SO	–	–
Underlying Event (S)	–	SO	SO	–	–
PDF, reweighting (S)	SO	SO	SO	SO	–

D0 $\nu\nu b\bar{b}$ Double Tag (DT) channels relative uncertainties (%)

Contribution	Top	$V + b\bar{b}/c\bar{c}$	$V+l.f.$	Dibosons	Multijet
Jet ID efficiency	2.0	2.0	2.0	2.0	–
Jet Energy Scale	2.1	1.6	3.4	1.2	–
Jet Energy Resolution	0.7	0.4	0.5	1.5	–
Vertex Conf. / Taggability	2.6	1.6	1.6	1.8	–
b Tagging	6.2	4.3	4.3	3.7	–
Lepton Identification	2.0	0.9	0.8	0.9	–
Trigger	2.0	2.0	2.0	2.0	–
Heavy Flavor Fractions	–	20.0	–	–	–
Multijet model	–	–	–	–	25
Cross Sections	10.0	10.2	10.2	7.0	–
Luminosity	6.1	6.1	6.1	6.1	–
Multijet Normalilzation	–	–	–	–	–
ALPGEN MLM pos/neg (S)	–	–	SO	–	–
ALPGEN Scale (S)	–	SO	SO	–	–
Underlying Event (S)	–	SO	SO	–	–
PDF, reweighting (S)	SO	SO	SO	SO	–

TABLE IX: Systematic uncertainties for the D0 $\ell b\bar{b}$ single tag (ST) and double tag (DT) channels. Systematic uncertainties are listed by name; see the original references for a detailed explanation of their meaning and on how they are derived. Uncertainties are relative, in percent on the event yield. Shape uncertainties are labeled with an “(S)”.

D0 $\ell b\bar{b}$ Single Tag (ST) channels relative uncertainties (%)						
Contribution	Multijet	Z+l.f.	Z + $b\bar{b}$	Z + $c\bar{c}$	Dibosons	Top
Jet Energy Scale (S)	–	3.0	8.4	10	3.3	1.5
Jet Energy Resolution (S)	–	3.9	5.2	5.3	0.04	0.6
Jet ID efficiency (S)	–	0.9	0.6	0.2	1.0	0.3
Taggability (S)	–	5.2	7.2	7.3	6.9	6.5
Z_{p_T} Model (S)	–	2.7	1.4	1.5	–	–
HF Tagging Efficiency (S)	–	–	5.0	9.4	–	5.2
LF Tagging Efficiency (S)	–	73	–	–	5.8	–
ee Multijet Shape (S)	53	–	–	–	–	–
Multijet Normalization	20-50	–	–	–	–	–
Z+jets Jet Angles (S)	–	1.7	2.7	2.8	–	–
Alpgen MLM (S)	–	0.3	–	–	–	–
Alpgen Scale (S)	–	0.4	0.2	0.2	–	–
Underlying Event (S)	–	0.2	0.1	0.1	–	–
Trigger (S)	–	0.03	0.2	0.3	0.3	0.4
Cross Sections	–	–	20	20	7	10
Normalization	–	1.3	1.3	1.3	8.0	8.0
PDFs	–	1.0	2.4	1.1	0.7	5.9

D0 $\ell b\bar{b}$ Double Tag (DT) channels relative uncertainties (%)						
Contribution	Multijet	Z+l.f.	Z + $b\bar{b}$	Z + $c\bar{c}$	Dibosons	Top
Jet Energy Scale (S)	–	4.0	6.4	8.2	3.8	2.7
Jet Energy Resolution(S)	–	2.6	3.9	4.1	0.9	1.5
JET ID efficiency (S)	–	0.7	0.3	0.2	0.7	0.4
Taggability (S)	–	8.6	6.5	8.2	4.6	2.1
Z_{p_T} Model (S)	–	1.6	1.3	1.4	–	–
HF Tagging Efficiency (S)	–	–	1.3	3.2	–	0.7
LF Tagging Efficiency (S)	–	72	–	–	4.0	–
ee Multijet Shape (S)	59	–	–	–	–	–
Multijet Normalization	20-50	–	–	–	–	–
Z+jets Jet Angles (S)	–	2.0	1.5	1.5	–	–
Alpgen MLM (S)	–	0.4	–	–	–	–
Alpgen Scale (S)	–	0.2	0.2	0.2	–	–
Underlying Event(S)	–	0.1	0.02	0.1	–	–
Trigger (S)	–	0.3	0.2	0.1	0.2	0.5
Cross Sections	–	–	20	20	7	10
Normalization	–	1.3	1.3	1.3	8.0	8.0
PDFs	–	1.0	2.4	1.1	0.7	5.9

TABLE X: The correlation matrix for the D0 analysis channels. Uncertainties marked with an \times are considered 100% correlated across the affected channels. Otherwise the uncertainties are not considered correlated, or do not apply to the specific channel. The systematic uncertainties on the background cross section (σ) and the normalization are each subdivided according to the different background processes in each analysis.

Source	$\ell\nu b\bar{b}$	$\nu\nu b\bar{b}$	$\ell\ell b\bar{b}$
Luminosity	\times	\times	
Normalization			
Jet Energy Scale	\times	\times	\times
Jet ID	\times	\times	\times
Electron ID/Trigger	\times	\times	\times
Muon ID/Trigger	\times	\times	\times
b -Jet Tagging	\times	\times	\times
Background σ	\times	\times	\times
Background Modeling			
Multijet Background			
Signal σ	\times	\times	\times